Nanoscale

PAPER

View Article Online
View Journal | View Issue

Cite this: *Nanoscale*, 2020, **12**, 14751

Anti-DLL4 VNAR targeted nanoparticles for targeting of both tumour and tumour associated vasculature†

Adam Leach,‡[a] Peter Smyth,‡[a] Laura Ferguson,[b] John Steven,[b] Michelle K. Greene,[a] Cristina M. Branco,[a] Aidan P. McCann,[a] Andrew Porter,[b,c] Caroline J. Barelle*[b] and Christopher J. Scott *[a]

Received 14th April 2020,
Accepted 28th June 2020

DOI: 10.1039/d0nr02962a

rsc.li/nanoscale

Whilst there is an extensive body of preclinical nanomedicine research, translation to clinical settings has been slow. Here we present a novel approach to the targeted nanoparticle (NP) concept: utilizing both a novel targeting ligand, VNAR (Variable New Antigen Receptor), a shark-derived single chain binding domain, and an under-investigated target in delta-like ligand 4 (DLL4). We describe the development of an anti-DLL4 VNAR and the site-specific conjugation of this to poly(lactic-*co*-glycolic) acid PEGylated NPs using surface maleimide functional groups. These nanoconjugates were shown to specifically bind DLL4 with high affinity and were preferentially internalized by DLL4-expressing pancreatic cancer cell lines and endothelial cells. Furthermore, a distinct anti-angiogenic effect endowed by the anti-DLL4 VNAR was evident in *in vitro* tubulogenic assays. Taken together these findings highlight the potential of anti-DLL4 targeted polymeric NPs as a novel therapeutic approach in pancreatic cancer.

Introduction

Over the last 15–20 years nanoformulations for both therapeutic and diagnostic applications have been increasingly investigated. Such delivery systems have the potential to maximise drug delivery to the requisite site, minimising off-target toxicities.[1] As potential chemotherapeutics, NPs may passively target tumours through the enhanced permeability and retention (EPR) effect, wherein leaky hypervasculature permits the extravasation of the nanosystem into tumour tissue and poor lymphatic clearance minimises removal.[2–4]

NPs can be further tailored by functionalizing their exterior with targeting ligands. Such ligands can be used to target an encapsulated therapeutic payload to the requisite site whilst through interaction with receptors and other molecules, targeting moieties can themselves impart biological function.[5–9] One potential targeting approach that has not yet been adequately investigated is that of using Variable New Antigen Receptors (VNARs).

VNARs are the smallest (11 kDa) naturally occurring independent binding domains in the vertebrate kingdom, playing an integral role in the adaptive immune system of cartilaginous fish.[10–12] Structurally, their characteristic protruding paratopes result in "canyon-binders", predisposed to access epitopes normally inaccessible to conventional biologics. This enables the generation of ligands possessing high binding efficacy and specificity.[13–18] Furthermore, scaled VNAR expression can be achieved cost-efficiently in non-mammalian systems whilst their inherent stability makes them ideal for chemically controlled orientated conjugation to NPs to provide an efficient display of binding paratopes.

In this work a VNAR against Delta-like ligand 4 (DLL4) is conjugated to therapeutic NPs in order to target their action to DLL4-overexpressing tumours. DLL4 is a haploinsufficient Notch1 ligand essential for embryonic vascular development and arteriogenesis.[19,20] Its specific role appears to be in the selection of tip cells during angiogenesis, resulting in appropriately-branched vasculature.[21,22] In vascular endothelial cells hypoxia stimulates the production of VEGF-A[23] which subsequently increases expression of DLL4 through binding to VEGFR2. Increased DLL4-Notch1 signalling then participates in the appropriate spatial selection of endothelial tip cells.[24] Structurally, DLL4 is a single-pass transmembrane protein,[25] befitting its role in Notch signalling requiring cell–cell contact.

While DLL4 expression is very low in normal adult endothelium, its overexpression has been observed in the tumour-

[a]*The Patrick G. Johnston Centre for Cancer Research, School of Medicine, Queen's University Belfast, Belfast, UK. E-mail: c.scott@qub.ac.uk*
[b]*Elasmogen Ltd, Aberdeen, UK. E-mail: caroline.barelle@elasmogen.com*
[c]*The Institute of Medical Sciences, University of Aberdeen, Aberdeen, UK*

†Electronic supplementary information (ESI) available. See DOI: 10.1039/d0nr02962a

‡These authors contributed equally.

associated endothelium of several cancers including bladder, breast, colon, kidney and brain, while expression is much lower or absent in nearby normal vasculature.[26–30] DLL4 overexpression is also observed in pancreatic ductal adenocarcinoma (PDAC), notably not just in tumour-associated vasculature but also in tumour cells themselves. Immunohistochemical staining of patient samples indicates >50% of PDAC samples have high DLL4 expression, falling to approximately 20% in peritumoural tissues.[32,34] This overexpression of DLL4 in the tumour bulk and vasculature presents an opportunity for selective localisation of DLL4-binding NPs, and any associated cargo, at the tumour site. High DLL4 expression in PDAC correlates with poor prognosis[31–34] suggesting a pro-carcinogenic role. DLL4 blockade is found to induce excessive sprouting of vasculature and to inhibit tumour growth,[35,36] while not causing the gastrointestinal toxicity observed with other Notch pathway inhibitors.[37,38] DLL4 expression is also a marker of cancer stem cells (CSCs). Preclinically, DLL4 blockade reduces EMT and the number of CSCs,[36,39] suggesting potential effects on PDAC recurrence and metastatic ability. As such DLL4 is an exciting target for NP therapies in PDAC, with potential therapeutic effects beyond simply enhancing selective NP localization.

Hard-to-treat cancers such as PDAC have a five-year survival rate of less than 4%; a shocking statistic that has remained virtually unchanged since the 1970s. Therefore new therapeutic strategies, such as DLL4 inhibition, are urgently required. Given the potential of using VNARs as NP targeting moieties we herein describe the formulation and assessment of a polymeric NP targeted against DLL4. Following determination of the physical characteristics of the NP system, the ability of the conjugated VNAR to bind recombinant DLL4 protein was assessed in an array of assays. Subsequently, the functionality of the VNAR-NP conjugate was assessed using *in vitro* cell based assays.

Results and discussion

Isolation and functional characterization of DLL4-specific VNAR E4-Fc

The DLL4 specific domain E4 was isolated from a synthetic VNAR library using phage display technology. The library was subjected to four rounds of solid phase selection and screened for clones cross-reactive to both human and murine DLL4. Binding clones were converted to an Fc format.[17] VNAR E4-Fc was chosen as a preferred lead due to an exquisite selectivity for human and murine DLL4 over the closely related ligand DLL1 (both human and murine), when assessed by ELISA (Fig. 1A).

The extracellular domain of human DLL4 is a single pass transmembrane protein containing 8 EGF repeats and a single DSL region. The Genentech clinical benchmark mAb, YW26.82, is known to bind an epitope within EGF like repeat number 2.[35] In order to narrow down the binding region (epitope) of VNAR E4-Fc and determine whether it was similar

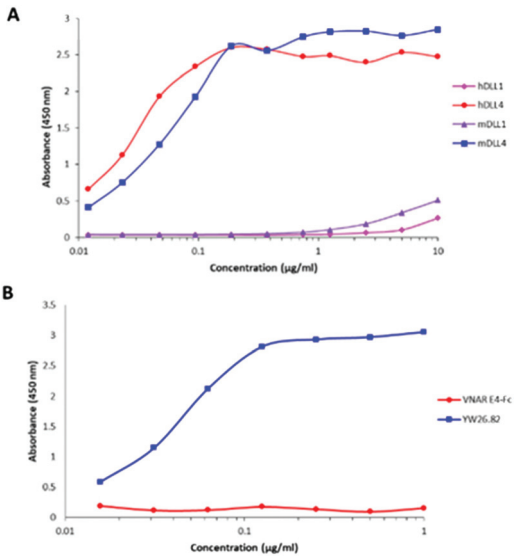

Fig. 1 Binding specificity and selectivity of VNAR E4-Fc. Binding ELISAs of (A) VNAR E4-Fc to human and murine DLL4 and the closely related ligand DLL1 and (B) binding of the VNAR E4-Fc and YW26.82 mAb to a truncated version of DLL4 displaying only DSL and EGF repeats 1–3.

to that of YW26.82, a truncated version of human DLL4 was expressed containing only the DSL and EGF repeats 1–3. Binding of VNAR E4 and mAb YW26.82 to the truncated DLL4 protein was assessed by ELISA (Fig. 1B). YW26.82 binds the truncated version as expected however, VNAR E4-Fc did not bind within this region, indicating an epitope distinct from YW26.82. This result also suggests that VNAR E4-Fc may bind a more membrane proximal epitope. This is likely to be the case as a result of both the smaller size of VNARs (~11 kDa in comparison to ~150 kDa for a mAb) and their diverse range of paratope topologies, which enable them to bind hidden or cryptic epitopes, inaccessible to conventional antibodies. The predisposition of VNARs to bind epitopes which are more membrane proximal has been reported previously for a VNAR that recognizes the ROR1 protein.[40]

Blockade of DLL4-Notch activity is known to induce hyper-sprouting (branching) through the stimulation and differentiation of an increased number of tip cells, leading to local regions of hypoxia and non-productive angiogenesis. Aberrant sprouting in a cancer setting therefore leads to increased vessel density, tumour hypoxia and attenuated tumour growth.[35,41] Given that the data indicated that VNAR E4 bound DLL4 through a distinct epitope to YW26.82, it was important to determine whether this would still translate into an altered sprouting phenotype. DLL4 blockade was assessed over a period of 7 days in a HUVEC fibrin bead-sprouting assay, and activity again compared with the clinical benchmark mAb YW26.82. Representative images from each treatment are shown in Fig. 2A. As previously reported, inhibition of the DLL4-Notch pathway by YW26.82 resulted in a hyper sprouting phenotype with multiple branch points on each sprout.[35] Interestingly, treatment with VNAR E4-Fc resulted in an

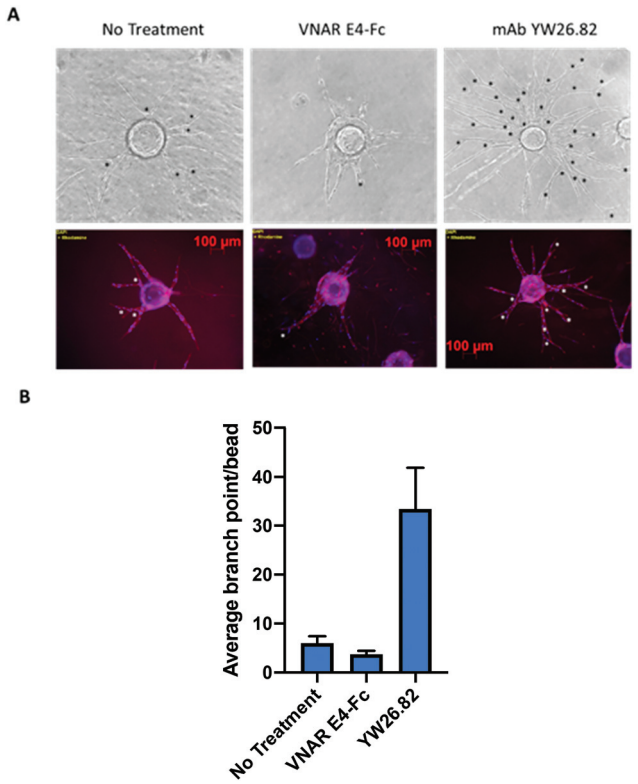

Fig. 2 DLL4 blockade by VNAR E4-Fc results in an alternative sprouting phenotype. (A) HUVEC coated beads in a fibrin matrix were cultured for 7 days in media only (no treatment) or supplemented with 250 nM VNAR E4-Fc or mAb YW26.82. The branch points of each sprout are indicated by a star. Representative images under phase contrast and confocal microscopy post F-actin staining are shown. (B) The number of branch points per bead were counted and a total of 10 beads were analysed per treatment (n = 3).

alternative sprouting phenotype with a reduced number of sprouts each with a noticeably thicker lumen (Fig. 2A). The number of branch points per bead were counted for each treatment (Fig. 2B). The addition of YW26.82 to HUVEC cells led to a significantly increased number of sprouts and branch points, and the converse was true for VNAR E4-Fc, further reinforcing the argument that DLL4 blockade by VNAR E4-Fc is *via* a novel epitope and/or mechanism.

Synthesis and characterization of VNAR-conjugated PLGA-PEG NPs

As an alternative to utilizing a Fc-fusion protein to increase VNAR binding avidity, conjugation to polymeric NPs was proposed as an approach to enhance paratope display. We have previously shown that using site-selective conjugation chemistries, formulations possessing high binding affinities can be generated.[42] Using a similar oil-in-water single emulsion evaporation approach, we successfully generated NPs incorporating a PEGylated stealth coat and a maleimide functionality to facilitate downstream site-selective conjugation to a free c-terminal cysteine engineered into the VNAR fragments. Upon assessment by DLS, these NPs were found to be approximately

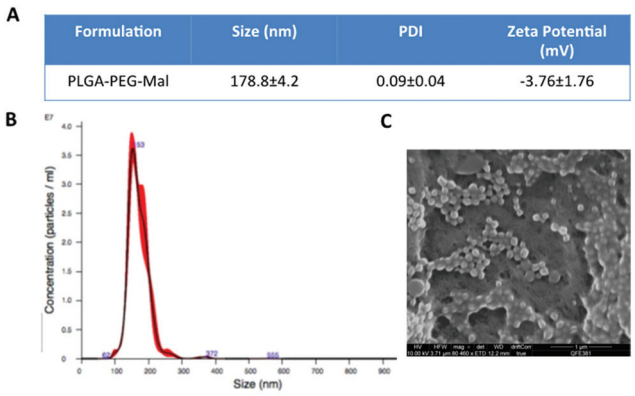

Fig. 3 Physical characterisation of PLGA-PEG-Mal polymeric NPs. PLGA-PEG-Mal polymeric NPs were formed using a single emulsion–solvent evaporation approach. The resulting nanostructures were physically assessed to ascertain their size and morphology by (A) DLS, (B) NTA and (C) SEM.

200 nm in diameter with a slightly negative zeta potential of −3 mV in PBS (Fig. 3A). Furthermore, the low polydispersity (0.1) suggested that a uniform monodisperse population of NPs had been generated by this strategy. The size and polydispersity parameters were further confirmed by NP tracking analysis (NTA) and scanning electron microscopy (SEM) (Fig. 3B and C). The stability of this formulation was then assessed over time. Isolated NPs were stored at a range of temperatures (−80, −20, 4, room temperature and 37 °C), before being resuspended in PBS and reanalyzed by DLS, revealing that physical characteristics remained largely unaltered (Fig. S1A–C†).

Evaluation of VNAR conjugated PLGA NPs binding to recombinant DLL4

To facilitate the conjugation of the anti-DLL4 VNAR, E4, to the maleimide moieties on the NP, the purified E4 VNAR was incubated with the NPs under gentle agitation for 2 h, allowing an 80% conjugation efficiency, equating to 8 μg protein per mg polymer formulation. As a control, a naive control VNAR, 2V, was also conjugated to the NPs. Conjugation levels between the two VNAR clones were noted to be comparable with both conjugated NPs also possessing similar physicochemical characteristics (Fig. 4A).

Analysis of VNAR-NP binding to DLL4 was initially confirmed by fluorescence-linked immunosorbent assay (FLISA), using microtiter plates coated with DLL4-Fc protein. In these experiments, the incorporation of rhodamine 6G in the NP afforded fluorescent measurement of NP binding. For E4 conjugated NPs specific binding to DLL4-Fc was significantly increased over that observed with the isotype control. 2V isotype control nanoconjugate binding response was found to be comparable to that of the nude, unconjugated NP (Fig. 4B).

To further assess the ability of the E4 VNAR-NP to recognize DLL4, SPR analysis was carried out using DLL4-Fc protein immobilized onto a carboxymethylated dextran chip. Samples were allowed to flow over the chip for 15 s with a flow rate of

A

Formulation	Size (nm)	PDI	Conjugation (ug/mg)	Conjugation Efficiency (%)
PLGA-PEG-Mal-E4	223.6±25.2	0.19±0.02	8.01±1.96	80.1±19.6
PLGA-PEG-Mal-2V	208.4±15.0	0.15±0.06	6.99±1.11	69.9±11.1

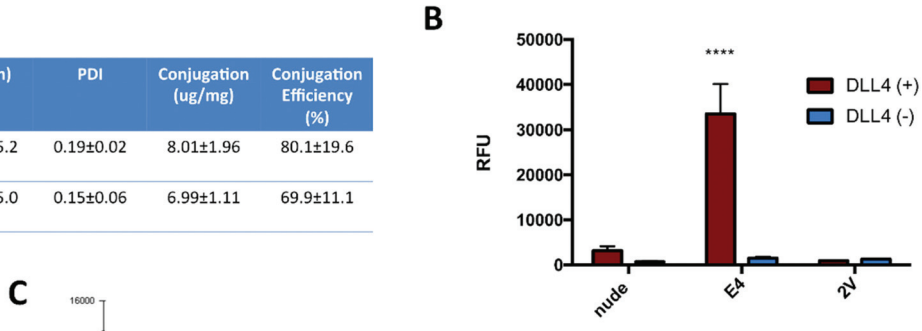

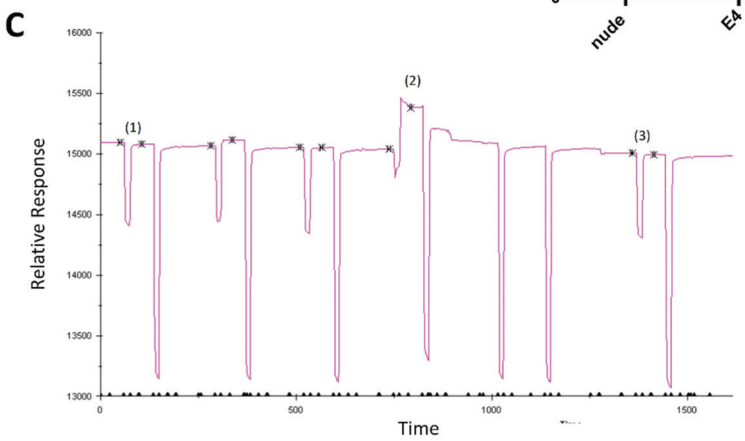

D

Formulation	Relative Response
(1) PLGA-PEG-Mal	-15.6
(2) PLGA-PEG-Mal-E4	341.6
(3) Clone E4 conjugation control	-12.4

Fig. 4 E4 (anti-DLL4) conjugated NPs bind specifically to recombinant DLL4 (A) size and PDI of E4 and 2V (isotype) conjugated PLGA-PEG-Mal NPs and amount of conjugated VNAR as measured by DLS and mBCA respectively. (B) FLISA assessment of DLL4 binding by nude, E4- and 2V-conjugated NPs. Assay performed in triplicate and data presented as mean of three independent experiments. Statistical significance was established by two-way ANOVA and Tukey's *post-hoc* test (****$p \leq 0.0001$). (C) PLGA-PEG-Mal polymeric NPs were incubated with anti-DLL4 clone E4 VNAR. Post-incubation, the ability of the NPs to bind DLL4 was determined by SPR. Data presented as representative SPR binding sensorgram and (D), corresponding details for relative binding response.

20 μL min^{-1}. Chip regeneration was conducted between each sample through the addition of sodium hydroxide solution (25 mM–50 mM) at 20 μL min^{-1} for 15 s. Using equalized amounts of NPs, we first demonstrated that binding of the nude control NPs to the immobilized DLL4 protein was negligible, whereas the E4 VNAR conjugated NPs showed markedly enhanced binding. To ensure that we were not simply measuring binding of free VNAR aggregates in our formulations, we also prepared conjugation controls wherein the VNAR was subjected to the same coupling and washing procedure in the absence of NPs. The lack of response in these samples confirmed that the binding observed with the VNAR-NPs was dependent on VNAR association with the NP, highlighting the success of the maleimide-cysteine conjugation approach (Fig. 4C and D).

The engineered C-terminal cysteine of the VNAR is expected to be the most amenable residue to electrophile conjugation. To highlight the advantageous nature of this site-specific coupling approach we compared it to conventional NHS-ester chemistry that has been widely employed during the construction of targeted nanoparticles to date. In the latter approach, conjugation to the NP occurs randomly at lysine residues throughout the VNAR structure. Whilst the coupling efficiency of the VNAR to the NP was similar using both chemistries (Fig. 5A), vastly superior antigen binding was observed with the maleimide chemistry. DLL4 binding, was noted to be ~6.5 times greater 30 s after sample addition for PLGA-PEG-Mal-E4 NPs compared to PLGA-PEG-NHS-E4 NPs, as determined by SPR, with similar findings observed using the FLISA approach (Fig. 5B–D). This highlights that the site-specific nature of the maleimide conjugation approach plays a critical role in antigen binding; indicating improved paratope accessibility due to controlled orientation of VNAR fragments on the NP surface.

To rule out the possibility that the E4 VNAR was simply adsorbed to the PLGA NP and not covalently attached, we then

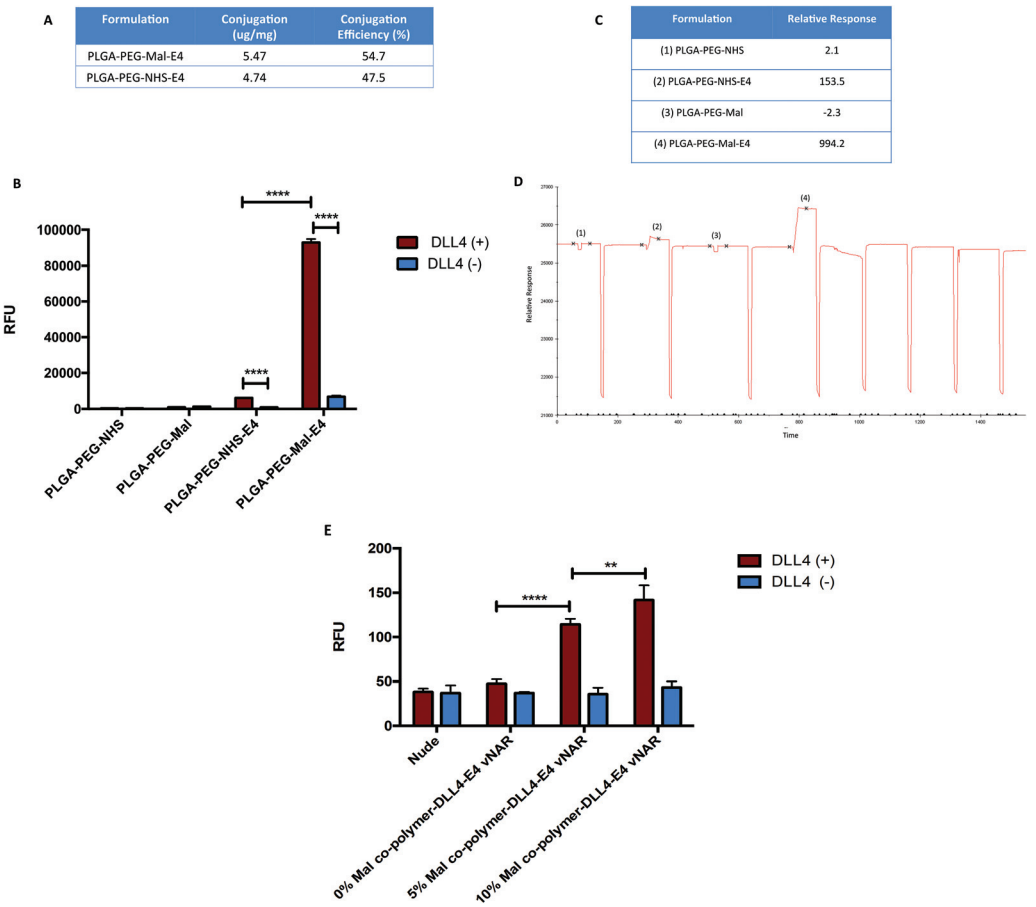

Fig. 5 Anti-DLL4 VNAR conjugation is maleimide dependent. Rhodamine 6G loaded PLGA-PEG-Mal and PLGA-PEG-NHS polymeric NPs were incubated with anti-DLL4 clone E4 VNAR. Post-incubation, NPs were assessed (A) in terms of the success of the conjugation reaction, as determined by mBCA. Rhodamine 6G loaded PLGA-PEG-NHS-E4 and PLGA-PEG-Mal-E4 NPs binding assessment *via* (B) FLISA method. Data expressed as mean ± standard deviation (SD). Representative of three independent experiments. Statistical significance was established by two-way ANOVA and Tukey's *post-hoc* test (****$p \leq 0.0001$). (C) Binding assessment of PLGA-PEG-Mal-E4 and PLGA-PEG-NHS-E4 NPs by SPR. Data presented as relative binding response with (D), corresponding SPR binding sensorgram details. Representative of three independent experiments. (E) Rhodamine 6G-loaded PLGA-PEG-Mal polymeric NPs possessing varying proportions of PLGA-PEG-Mal copolymer, were conjugated with anti-DLL4 clone E4 VNAR and binding assessed by FLISA. Data expressed as mean ± standard deviation (SD). Representative of two independent experiments. Statistical significance was established by two-way ANOVA and Tukey's *post-hoc* test (**$p \leq 0.01$; ****$p \leq 0.0001$).

explored the binding characteristics of NPs employing different proportions of the maleimide functionalized PLGA-PEG-Mal copolymer. Incubations with these varying formulations revealed that incorporation of increasing amounts of the maleimide functionalized copolymer yielded increasing binding; importantly, when 0% of the PLGA-PEG-Mal was used in the formulation, binding of the NP to the DLL4 coated plates was directly comparable to controls (Fig. 5E). This demonstrates that the binding of these NPs to DLL4 is dependent on the site-specific, maleimide-cysteine conjugation of the VNAR to the NPs.

To further illustrate the specificity of the binding interaction between the anti-DLL4 VNAR targeted NPs and their cognate antigen, FLISA binding was assessed following blocking of the NP-bound VNAR paratope with free DLL4-Fc (Fig. S2A†) or the plate-bound DLL4-Fc epitope with free anti-DLL4 VNAR (Fig. S2B†). In both cases reduction in binding of the anti-DLL4 NPs highlights the specificity of the interaction between the targeted VNAR NP and its cognate antigen (DLL4). In order to assess the suitability of the VNAR-NP conjugates for use in a biological setting, antigen binding was assessed *via* FLISA in biological media. Encouragingly, significantly enhanced binding of VNAR-targeted NPs was maintained over non-targeted nude and isotype control NPs (Fig. S3†).

Evaluation of anti-DLL4 NPs to target DLL4 positive tumour cells

Having demonstrated the selective binding of the E4-conjugated NPs to DLL4, suitable cell models were sought for more biologically relevant investigation of the behaviour of the anti-DLL4 NPs.

While DLL4 is classically considered an endothelial ligand it has been shown that its expression is not restricted to the vasculature and is indeed found within the tumour bulk where

its signalling through Notch1 seems to promote maintenance of CSCs and EMT, for example.[36,39,43] Therefore it is valuable to look at the effects of E4-conjugated NPs on pancreatic cancer cells (*i.e.*, cancer cell lines) to ascertain if anti-DLL4 NPs may be of benefit in targeting to the tumour bulk. Published data indicates that several PDAC cell lines. Including MIA PaCa-2[43] and PANC-1,[44] express DLL4.

As such, DLL4 expression was investigated in MIA PaCa-2 and PANC-1 cells by western blot and flow cytometry and both were found to be DLL4 positive (Fig. 6A–D). The uptake of rhodamine 6G VNAR-conjugated NPs was assessed by plate reader in MIA PaCa-2 and PANC-1 cells (Fig. 6E and F). The small yet significant enhancement in uptake of DLL4-targeted over isotype-control NPs indicates a potential role for using the E4 VNAR-NP as a platform for targeted drug delivery to the tumour bulk.

Evaluation of anti-DLL4 NPs to target and modulate the tumour vasculature

In addition to delivering a therapeutic payload to the tumour bulk it may also be advantageous to target the tumour vasculature. Therefore the next series of studies assessed the inherent functionality of the anti-DLL4 VNAR, when conjugated to the NP surface, against endothelial cells. Given that DLL4 is classically expressed in the vascular endothelium, HUVECs were therefore employed as a cell model. In agreement with the literature, synergistic upregulation of DLL4 was observed in these cells upon co-stimulation with VEGF and FGF (Fig. 7A and B).[29] Internalization of rhodamine-loaded E4-conjugated NPs was assessed in DLL4-positive HUVEC cells. NPs and cells were incubated together for 30 min at 4 °C, an approach well characterised to discriminate between NP absorption and active uptake *in vitro*.[45] Unbound NPs were then removed by washing before 3 h incubation at 37 °C to enable the cellular uptake of surface bound NPs. Greater uptake of the E4-functionalized NPs when compared to the nude NPs highlights the impact of the anti-DLL4 VNAR in facilitating increased NP internalization in DLL4 expressing cells (Fig. 7C).

As a further illustration of NP targeting, we prepared our NPs encapsulating the cytotoxic agent camptothecin (CPT) (Fig. S4†) and incubated these with the stimulated HUVECs for

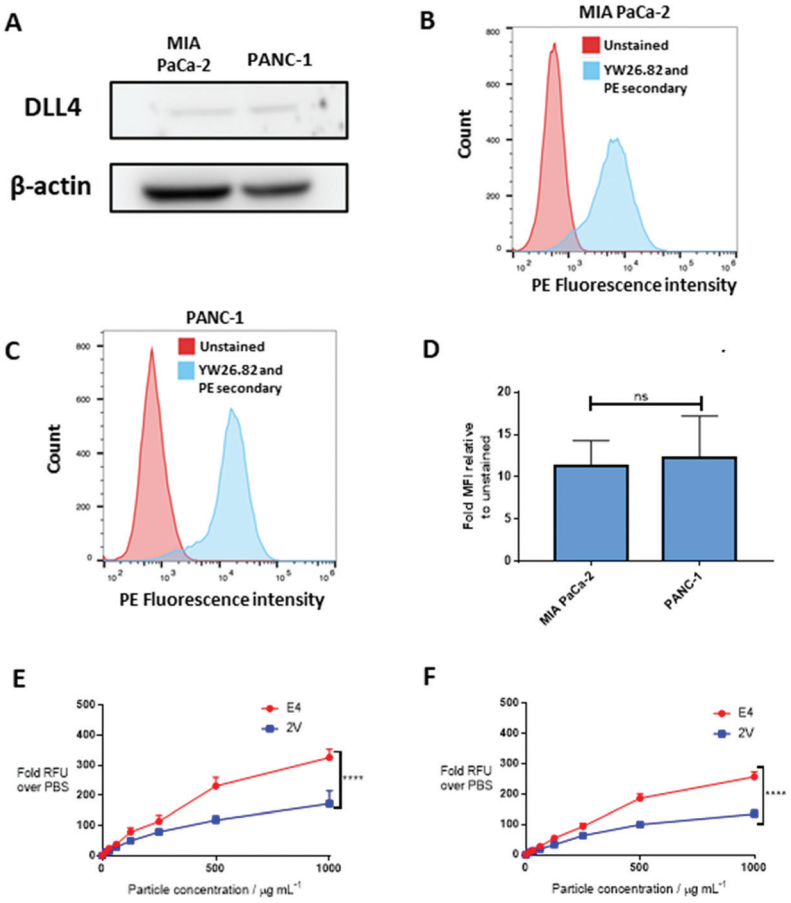

Fig. 6 Basal expression of DLL4 in PDAC cell lines correlates with enhanced uptake of anti-DLL4 VNAR conjugated PLGA-PEG-Mal NPs (A) western blot of lysates of MIA PaCa-2 and PANC-1 cells ($N = 4$). (B–C) Representative histograms of cell fluorescence intensity for MIA PaCa-2 and PANC-1 cells either unstained or stained with YW26.82 and an anti-human PE-conjugated secondary antibody (D) mean fluorescence intensity measurements (relative to unstained control). Significance assessed by unpaired *t*-test (ns $p > 0.05$) ($N = 3$) (E–F) uptake of fluorescent NPs into MIA PaCa-2 and PANC-1 cells respectively. Significance was assessed by two-way ANOVA and Tukey's *post-hoc* test (****$p < 0.0001$).

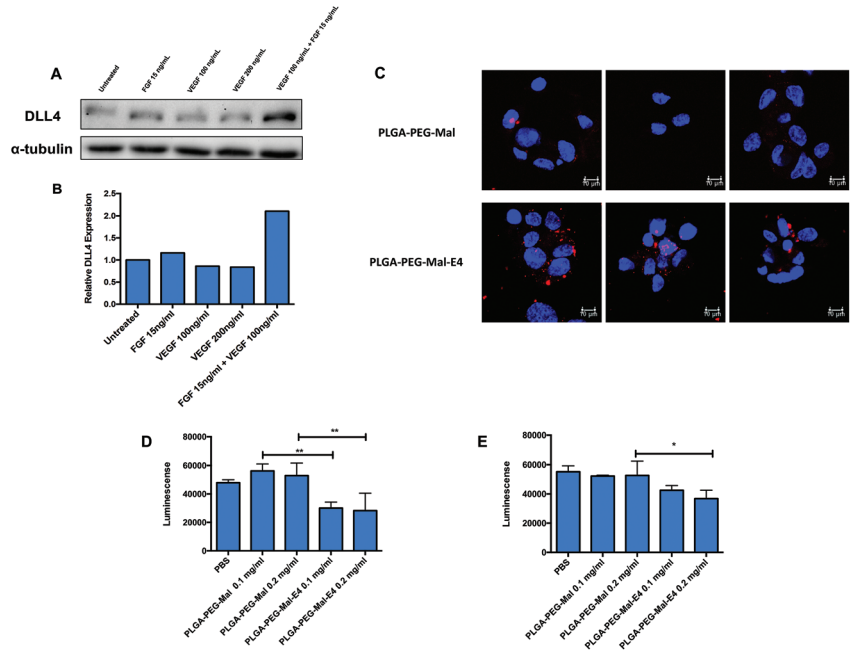

Fig. 7 Anti-DLL4 conjugated vNAR NPs enhance payload delivery to DLL4 expressing endothelial cells (A) HUVECs were treated with FGF and/or VEGF for 24 h. Following treatment, cells were lysed and DLL4 expression validated by western blot. α-Tubulin was used as a loading control. (B) Densitometry quantification of western blot DLL4 expression levels. (C) HUVEC cells (pre-stimulated with FGF and VEGF) were treated with either rhodamine 6G loaded PLGA-PEG-Mal or PLGA-PEG-Mal-E4 NPs for 3 h, then washed, fixed and nuclear regions stained with DAPI. Cells were subsequently imaged by confocal microscopy to assess formulation uptake. Three representative images per treatment group are shown. Scale bars = 10 μm. (D) HUVEC cells stimulated with VEGF/FGF were treated with CPT-loaded NPs for 1 h at 4 °C and cell viability was assessed 24 h and (E) 48 h post treatment *via* CellTiter-Glo®. Cells were treated with either 0.1 mg mL^{-1} or 0.2 mg mL^{-1} NP treatments, corresponding to 0.22 μg mL^{-1} or 0.44 μg mL^{-1} CPT respectively. Representative of two independent experiments. Statistical significance was established by one-way ANOVA and Tukey's *post-hoc* test (*$p \leq 0.05$; **$p \leq 0.01$).

1 h at 4 °C, before washing and replacing with fresh media. Cells were treated with either 0.1 mg mL^{-1} or 0.2 mg mL^{-1} NP treatments, corresponding to 0.22 μg mL^{-1} or 0.44 μg mL^{-1} CPT respectively. Measurement of cell viability at 24 and 48 h highlighted a significant decrease in cell viability for the VNAR-targeted NPs over non-targeted (nude) controls (Fig. 7D and E). By using anti-DLL4 VNARs as targeting agents for NPs there is therefore an opportunity to enhance the efficacy of chemotherapeutics within the tumour and its associated DLL4 positive neovasculature.

Given the endogenous function of DLL4 in angiogenesis it would be expected that DLL4 blockade by VNAR NPs would impact angiogenic signalling in the absence of any other therapeutic payload, we investigated the effect of E4-conjugated NPs in a tubulogenesis assay using HUVECs. In addition to growth factor stimulation, DLL4 expression is upregulated under hypoxic conditions. This upregulation under hypoxia is in accordance with previous observations in endothelial cells showing HIF-1α mediated transcriptional induction under hypoxia.[46,47] Such conditions are frequently found in the tumour microenvironment, and were therefore used here to replicate physiologically relevant enhancement of DLL4 expression (Fig. 8A). Following treatment with E4-conjugated NPs there was a marked difference in HUVEC tube phenotype (Fig. 8B and C). Quantification revealed no significant difference in branching interval between E4 NP treatments at 100 and 500 nM of NP-bound VNAR, indicating that anti-DLL4 effect of the E4 NPs was saturating under the assay conditions at 100 nM. Free E4 VNAR was also compared to NP bound VNAR at 100 nM (Fig. 8D and E). NP-bound VNAR decreased total mesh area significantly more than free VNAR, which may be due to the avidity effect of the multivalent NP *versus* the monovalent free VNAR. This change in HUVEC phenotype was similar to that observed following treatment with E4-Fc (Fig. 2). Again nascent branches did not extend/continue to grow.

This effect may be justified by the VNAR ligand used here. As previously shown, E4 appears to bind an epitope distinct from that of the mAb YW26.82. The unique constrained structure of VNARs are more able to bind membrane proximal epitopes, inaccessible to conventional antibodies. This may impart distinct conformational and functional changes upon the cognate antigen. Further structural analysis is required to fully elucidate the nature of the binding interaction between E4 and DLL4. However, the impact on tubulogenesis seen here, with inhibition of tube network formation observed following treatment with E4-NP, appears an exciting anti-angiogenic approach. Conjugation of VNARs to NP surfaces has the potential to broaden their therapeutic applications.

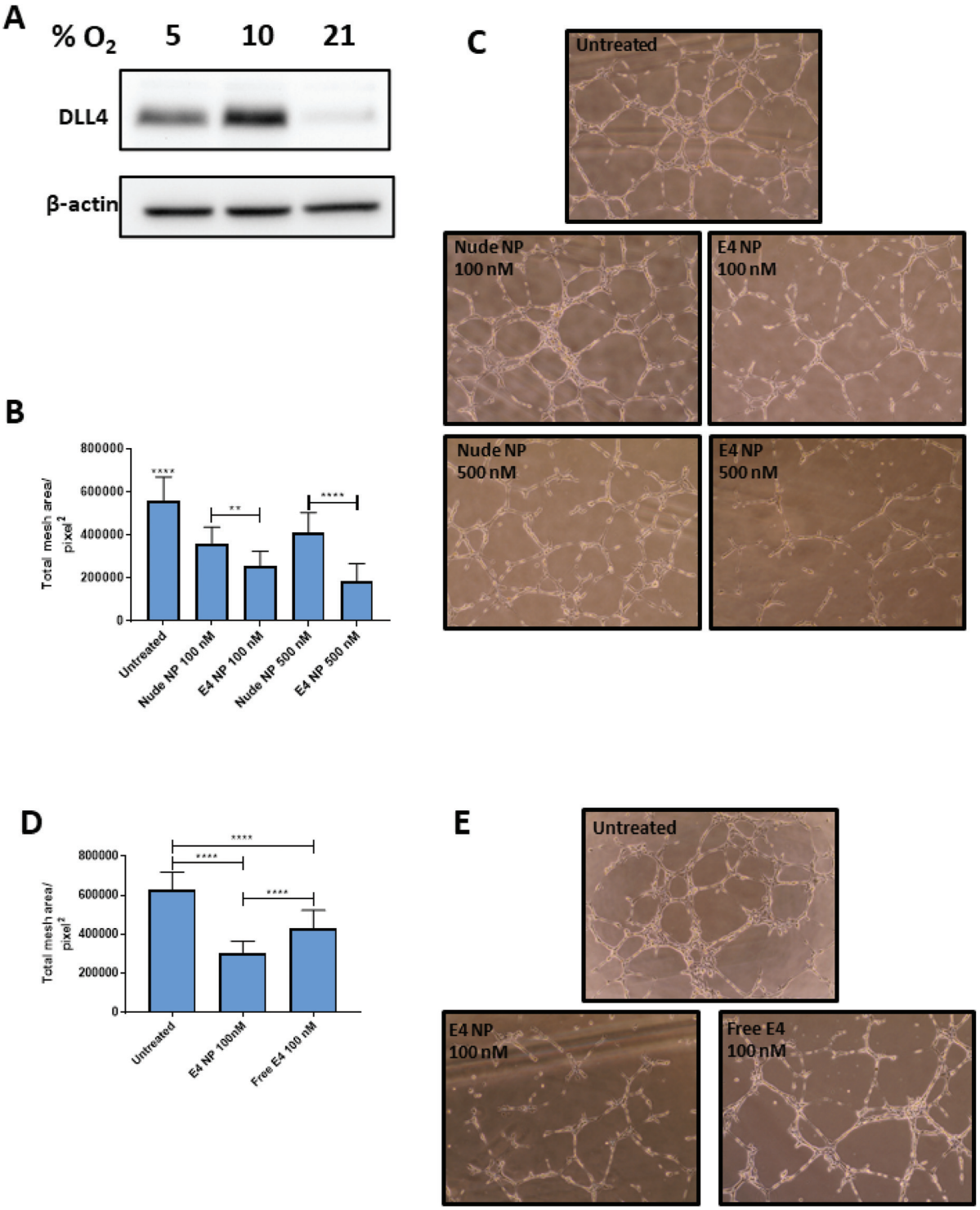

Fig. 8 HUVEC tube morphology is altered upon treatment with anti-DLL4 VNAR conjugated NPs (A) Representative DLL4 western blot of lysates derived from HUVECs cultured under varying oxygen conditions (5, 10 or 21% oxygen), β-actin used as loading control (B) quantification of total mesh area from the below phase contrast images using Angiogenesis Analyzer FIJI plugin. Data pooled from 3 independent experiments and normalized to untreated control. Statistical significance determined by two-way ANOVA (**$p < 0.01$, ****$p < 0.0001$). (C) Representative 10× phase-contrast images of HUVECs taken 6 hours after seeding with no treatment (untreated), E4 NPs (100 or 500 nM of NP-bound VNAR) or a matched polymer concentration of nude NP. (D) Quantification of total mesh area from the below phase contrast images using Angiogenesis Analyzer FIJI plugin. Data pooled from 3 independent experiments and normalized to untreated control. Statistical significance determined by two-way ANOVA (****$p < 0.0001$). (E) Representative 10× phase-contrast images of HUVECs taken 6 hours after seeding with no treatment (untreated), E4 NPs (100 nM of NP-bound VNAR) or free E4 (100 nM).

Conclusions

In summary we have demonstrated the potential application of anti-DLL4 targeted NPs as therapeutics in pancreatic cancer. Not only do these permit targeted delivery of nano-encapsulated cargo to the tumour bulk, but they also inhibit angiogenic DLL4-Notch1 signalling in models of the tumour vasculature. This inhibition may be *via* the recognition, by the E4 VNAR, of a membrane proximal epitope that delivers a novel inhibitory phenotypic change to growing cells, that in turn could translate into enhanced therapeutic potency *in vivo*. Whilst *in vivo* models are now clearly required to fully elucidate the potential of these NPs, they display promise particularly when one considers the current dearth of treatment options for life-shortening and aggressive solid-tumours such as those found in pancreatic cancer.

Experimental

VNAR phage display library screening

VNAR E4 was isolated from a synthetic VNAR library containing 100 billion unique clones. Four rounds of solid phase, phage display antigen selections were carried out as described previously[18] using MaxiSorp immunotubes (Nunc) coated with 10–4 μg ml^{-1} rhDLL4 (recombinant human) in PBS pH 7.4. Outputs from each selection round were screened for specificity to human and murine DLL4 (1 μg ml^{-1} in PBS coating concentration) by monoclonal phage and periplasmic extract ELISAs. Phage binders were detected using HRP-conjugated anti-M13 antibody (Stratech Scientific), and periplasmic protein was detected using an HRP-conjugated anti-His antibody (Sigma-Aldrich).

VNAR E4 ACA version design, expression and purification

Full details have been detailed previously.[42] An Alanine-Cysteine-Alanine (ACA) motif was inserted in the C-terminal region of VNAR E4 to facilitate site-specific NP conjugation. E4 ACA was cloned into the pIMS147 prokaryotic expression vector and solubly expressed in *E. coli* TG1 following 1 mM IPTG induction for 4 h at 30 °C, 250 rpm. E4 VNAR protein was released after osmotic shock (20% w/v sucrose, 100 mM Tris HCl pH7.6, 5 mM EDTA). His-tagged VNAR E4 was purified from the supernatant using Ni^{2+} IMAC resin and collected in a chromatography column. Bound protein was washed with 1×PBS containing 10 mM Imidazole and eluted with 10 ml of 250 mM Imidazole, pH 8. Post batch IMAC purification, VNAR E4 was subject to Anion Exchange chromatography. The fractions containing VNAR E4 ACA were pooled and buffer exchanged to 1×PBS, pH 7.4. Protein concentration was determined using the A280 spectrophotometer.

HUVEC fibrin bead sprouting assay

Fibrin gel angiogenesis assays were performed in a 24 well optical plate as described previously.[48] In brief, Cytodex 3 microcarrier beads (Amersham) were coated with HUVEC cells at a concentration of 400 cells per bead for 4 hours at 37 °C and allowed to adhere overnight. Approximately 250 HUVEC coated beads per well were embedded in 2 mg ml^{-1} fibrin gel and catalyzed by the addition of 0.625 U ml^{-1} thrombin (Sigma-Aldrich, UK). NHLF (20 000 cells per well) were seeded on top of each clot in EGM-2 medium supplemented with the indicated angiogenesis inhibitor (250 nM VNAR E4-Fc and YW26.83 benchmark mAb). The medium plus treatments were refreshed every other day and the experiment terminated at day 7 with the addition of 2% paraformaldehyde (PFA), for 1 h at 37 °C, followed by overnight incubation at room temperature. Assays were quantified using phase-contrast microscopy or confocal fluorescent microscopy after staining for polymeric F-actin.

NP formulation

NPs were synthesized *via* a standard single emulsion evaporation methodology. Briefly, PLGA 502H (15 mg) and PLGA-PEG-Mal (5 mg) (or PLGA-PEG-NHS (5 mg)) were dissolved in 1 ml of dichloromethane and added dropwise *via* a 25G needle into an aqueous phase (7 ml) comprised of 2.5% (w/v) polyvinyl alcohol in 2-(*N*-morpholino)ethanesulfonic acid (MES) buffer (pH 5). Emulsion formation was instigated through pulsed sonication for 90 seconds on ice. The resulting emulsion was then stirred overnight to permit solvent evaporation. Three sequential centrifugation wash steps were then performed at 20 000*g* in PBS for a total of 60 min. The final NP pellet was re-suspended as required in PBS.

1% (w/w) rhodamine 6G (Sigma-Aldrich, UK) was added into the organic phase in order to produce fluorescently labeled NPs for use in binding assays. Camptothecin (CPT) loaded NPs were formulated *via* the addition of CPT 0.50% (w/w). Briefly, for each 20 mg polymeric NP batch, CPT (10 μL of a 10 mg mL^{-1} stock solution in DMSO) was added to the DCM organic phase and mixed. This solution was then injected into the aqueous phase as detailed above. Loaded nanoparticles were purified *via* three sequential centrifugation wash steps performed at 20 000*g* in PBS for a total of 60 min at 4 °C.

NP functionalization

VNAR was conjugated to the exterior of the PLGA-PEG-Mal NP *via* the formation of a stable thioether bond. Briefly, 1% (w/w) VNAR was added to the NPs (1 mg) and gently agitated for 2 h at room temperature. After the conjugation reaction time had elapsed, unbound VNAR was removed *via* centrifugation at 16 900*g* for 20 min at 4 °C. NPs were then collected and re-suspended as required.

Success of NP functionalization was determined by microbicinchoninic acid protein assay (micro BCA Protein Assay Kit, Thermo Scientific Pierce, UK) as per manufacturer's directions. Conjugated VNAR was quantified *via* comparison to standards comprised of known concentrations of VNAR added to nude NPs.

NP formulation assessment

Post-formulation NPs were assessed in terms of size (mean particle size Zave), polydispersity index (PDI) and zeta potential (NanoBrook Omni, Brookhaven Instruments Corporation, US). Measurements were conducted, in triplicate, with NPs resuspended at 0.1 mg ml^{-1} in deionised water. Additional size analysis of unconjugated NPs was performed using NP tracking analysis (NTA, Malvern NS300). In order to assess the stability of the formulation, pelleted NPs were stored in a variety of conditions (−80, −20, 4, room temperature and 37 °C), before being resuspended in PBS and reanalyzed by DLS at predetermined intervals over the course of 28 days.

Scanning electron microscopy

NPs suspended in water (5 mg ml^{-1}) were added to double-sided copper tape, fixed to an aluminium stub and allowed to dry. NPs were then sputter coated with gold and imaged using an FEI Quanta 250 FEG – Environmental Scanning Electron Microscope (E-SEM).

Surface plasmon resonance

NP binding was assessed *via* Surface Plasmon Resonance (SPR). All experiments were conducted at 25 °C on a Biacore Q instrument. HBS-EP running buffer (GE Healthcare) was also used throughout. A carboxymethylated dextran CM5 sensor chip (GE healthcare) was initially activated with 0.4 M EDC and 0.1 M NHS enabling chip functionalisation with 20 μg ml^{-1} recombinant human DLL4 Fc chimera protein (Sino Biological) *via* carbodiimide chemistry. DLL4 Fc was prepared in a 10 mM sodium acetate buffer at pH 4.5. Following Fc addition 1 M ethanolamine hydrochloride (pH 8.5) was used to quench remaining NHS esters. Chip activation, functionalization and subsequent quenching solutions were permitted 7 min chip contact time with flow rate maintained at 10 μl min^{-1}. NPs, suspended in HBS-EP running buffer were added at the requisite concentration at 20 μL min^{-1} for 15 s. Chip regeneration following sample injection was achieved *via* the addition of sodium hydroxide solution (25 mM–50 mM) at 20 μL min^{-1} for 15 s. Sensorgrams obtained illustrate binding responses in absolute RU. Data presented as response relative to baseline is the difference in RU 10 s prior to and 30 s after sample addition.

Fluorescence-linked immunosorbent assay (FLISA)

Human DLL4 Protein (Fc Tag) (Sino Biological) was immobilized on a high-binding black plate (Greiner Bio-One) at 0.5 μg ml^{-1} in PBS and left overnight. The plate was washed three times in 0.1% PBST to remove unbound DLL4-Fc and blocked for 1 h in 1% BSA in PBS. Following this, 0.1% PBST washes were conducted as before, rhodamine loaded NP sample added and left for 2 h at room temperature. Again, the plate was washed to remove unbound NP before the addition of acetonitrile : DMSO (1 : 1) to lyse the NPs and subsequent assessment of binding *via* fluorescence (526/555).

Cell-line culture

Human umbilical vein endothelial cells (HUVEC) and normal human lung fibroblasts (NHLF) were purchased from Lonza and were maintained in the EGM-2 and FGM-2 bullet kits respectively. Human Umbilical Vein Endothelial Cells (HUVEC) were also obtained from Caltag Medsystems and cultured in Human Large Vessel Endothelial Cell Growth Medium Package (Caltag Medsystems) or endothelial cell growth medium (ECGM) consisting of low glucose DMEM : F12 with 1% penicillin/streptomycin, 1% nonessential amino acids, 2 mM sodium pyruvate, buffered with 20 mM HEPES and containing 20% FCS (Gibco), 20 μg ml^{-1} Heparin (Sigma), and 75 μg ml^{-1} endothelial mitogens (Merck). MIA PaCa-2 and PANC-1 cells were acquired from ATCC and cultured in high glucose DMEM supplemented with 10% FCS, 1% sodium pyruvate and 1% penicillin/streptomycin.

Cell lysis and BCA assay

Cells from 90 mm culture dishes were detached by scraping in 200 μL ice-cold PBS, then pelleted by centrifugation and resuspended in 100 μL RIPA lysis buffer supplemented with protease inhibitor cocktail tablet (Roche, UK, 1 tablet per 50 mL buffer). The cell suspension was kept on ice for 30 min and vortexed at regular intervals before centrifugation at 20 000*g* for 10 min at 4 °C. On the completion of the centrifugation the whole cell lysate was retrieved from the supernatant and protein content quantified by bicinchoninic acid (BCA) assay (Pierce, UK).

SDS-PAGE and western blotting

Lysates were denatured in X5 Laemmli Buffer at 95 °C for 10 min before separation by SDS-PAGE (8%). On the completion of protein separation proteins were transferred onto a polyvinylidene fluoride membrane (Millipore, UK) by semi-dry blotting. The membrane was subsequently blocked (5% w/v milk in TBS-Tween) for, at least, 1 h.

For VEGF/FGF stimulated HUVECs under hyperoxic conditions. Primary antibodies were added overnight at 4 °C. Primary antibodies used were rat anti-α-tubulin (1 : 10 000) (ab6160, Abcam, UK) and rat anti-human/mouse DLL4 (1 : 500) (mab1389, R&D systems). Following primary antibody incubation the membrane was washed in TBS-T and incubated with the appropriate secondary, rabbit anti-rat HRP conjugate (1 : 40 000) (ab102199, Abcam, UK), for 1 h. The membrane was washed using TBS-T, before addition of chemiluminescent substrate for 5 min and imaging of bands using a BioRad Molecular Imager ChemiDoc XRS+ Imaging System (BioRad, USA).

For HUVECs cultured in physiological oxygen tensions. Anti-DLL4 primary was 2589 (Cell Signalling Technology, 1 : 1000), anti-β-actin primary was A2228 (Sigma-Aldrich, 1 : 5000 dilution). Post-primary antibody incubation the membrane was washed in PBST (3 × 10 minutes) and incubated with the appropriate HRP-conjugated secondary antibody (Cell Signalling Technology, 1 : 2000 dilution) at room temperature

for 1 h before further PBST washing. Western Lightning ECL Plus substrate was added and chemiluminesence detected (G-Box, SynGene).

Surface DLL4 detection by flow cytometry

YW26.82 (human anti-DLL4 primary antibody), was expressed by John Steven and Laura Ferguson (Elasmogen Ltd). PE-conjugated goat anti-human IgG secondary antibody was obtained from eBioScience (Thermo-Fisher Scientific).

Cells were seeded (1×10^6) in a P90 and allowed to adhere overnight. After washing once with PBS cells were detached by addition of 0.1% EDTA-PBS (5 mL, 37 °C, 10 minutes). Detached cells were transferred to a 15 mL tube, cold 5% PBS-FCS (5 mL) added and cells pelleted (200*g*, 5 minutes, 4 °C), from this point onwards cells and all buffers were chilled on ice. The cell pellet was resuspended in PBS-FCS (5 mL) and divided between 4 new 15 mL tubes. Each sample was pelleted again and resuspended in PBS-FCS (300 μL) and YW26.82 (1 μg, 3.3 μg mL^{-1} final concentration) added to the appropriate tube and incubated (30 minutes, dark, 4 °C). PBS-FCS (5 ml) was then added to each tube and cells were pelleted, this was repeated once more before cells were resuspended in PBS-FCS (300 μL) and secondary antibody added (1 μg, 3.3 μg mL^{-1} final concentration) and incubated (20 minutes, dark, 4 °C). Cells were pelleted and washed twice before resuspension and fluorescence analysis with at least 10 000 events collected per sample (FL2 laser, PE-A detection channel, BD Accuri C6).

PLGA-PEG-Mal-VNAR NP confocal microscopy

HUVEC cells were seeded at 20 000 per well on an eight-well glass culture slide (BD Falcon) and allowed to adhere overnight. To upregulate DLL4 expression, cells were stimulated with FGF and VEGF for 24 h. In order to assess the uptake of nude and VNAR-targeted NPs, cells were serum starved in serum-free media for 3 h before treating with PLGA-PEG-Mal NPs (0.5 mg ml^{-1}). Cells were incubated at 4 °C for 30 min, washed in PBS (3×) and incubated at 37 °C for a further 3 h. On the completion of the treatment period, cells were washed with PBS (3×), treated with acid strip buffer (50 mM glycine, 150 mM NaCl in PBS, pH 3) for 5 min, washed in PBS (3×) and fixed with 4% w/v paraformaldehyde in PBS for 20 min. Following further washes in PBS (3×), cells were permeabilized with 0.5% v/v Triton X-100 in PBS for 5 min. Cells were then washed with PBS (3×) and coverslips added post application of Vectashield antifade mounting medium with DAPI (Vector Laboratories). Images were captured using a Leica SP8 confocal microscope (Leica, UK) *via* a HCX PL APO 1.4–0.6NA 63× oil immersion objective zoomed 1–4× with a 1024 × 1024 frame and 400 Hz scan speed. Fluorescent images were attained post excitation with a UV emitting diode (405 nm) and argon (488 nm); DPSS (561 nm); or HeNe (543 nm, 594 nm and 633 nm) lasers as required. Images presented in the same panels were acquired using standardized settings and parameters. Image analysis was conducted using Leica LAS X software (Leica, UK).

Cell viability assay

Cell viability was assessed *via* CellTiter-Glo (CTG) assay (Promega). HUVEC cells were seeded in 96-well plates at 1500 cells per well and allowed to adhere. HUVEC cells were stimulated with VEGF/FGF 24 h post seeding. Cells were subsequently treated with NP formulations (48 h after seeding) for 1 h or 10 min at 4 °C before replacement of media and incubation at 37 °C. After the incubation period, CellTiter-Glo assay was performed as per manufacturers instructions. Luminescence was measured (Biotek Synergy 2) and viability of treated cells expressed relative to that of control cells.

HUVEC tubulogenesis assay

10 μL of growth factor reduced Matrigel (Corning) was added to the lower well of a 15-well tissue-culture treated Angiogenesis μ-slide (Ibidi) and allowed to polymerise for 2 hours. 3000 HUVECs at around 70% confluency and passage <12 were then seeded in 50 μL of treatment containing media on top of the Matrigel disc in the upper chamber of each well. Networks of tubes were allowed to form for 5–6 hours and imaged *via* phase-contrast microscopy (EVOS, 10×).

Conflicts of interest

There are no conflicts to declare.

Acknowledgements

The authors acknowledge the Engineering and Physical Sciences Research Council (EPSRC) (S3802ASA) and the generous support of the Martin Family Foundation for funding the Ph.D. studentships of P. S. and A. L., respectively. This work was also partially funded through a US-Ireland R&D Partnership grant awarded by HSCNI (STL/5010/14), Medical Research Council UK (MC_PC_15013), and the Biotechnology and Biological Sciences Research Council (BBSRC) (BB/R009112/1).

References

1 S. Jain, A. S. Doshi, A. K. Iyer and M. M. Amiji, *J. Drug Targeting*, 2013, **21**, 888–903.
2 Y. Matsumura and H. Maeda, *Cancer Res.*, 1986, **46**, 6387–6392.
3 F. Danhier, *J. Controlled Release*, 2016, **244**, 108–121.
4 R. K. Jain and T. Stylianopoulos, *Nat. Rev. Clin Oncol.*, 2010, **7**, 653–664.
5 D. Goren, A. T. Horowitz, D. Tzemach, M. Tarshish, S. Zalipsky and A. Gabizon, *Clin. Cancer Res.*, 2000, **6**, 1949–1957.
6 W. C. Chen, G. C. Completo, D. S. Sigal, P. R. Crocker, A. Saven and J. C. Paulson, *Blood*, 2010, **115**, 4778–4787.

7 D. Shan, J. Li, P. Cai, P. Prasad, F. Liu, A. M. Rauth and X. W. Wu, *Drug Delivery Transl. Res.*, 2015, **5**, 15–26.
8 O. C. Farokhzad, J. Cheng, B. A. Teply, I. Sherifi, S. Jon, P. W. Kantoff, J. P. Richie and R. Langer, *Proc. Natl. Acad. Sci. U. S. A.*, 2006, **103**, 6315–6320.
9 D. Schmid, F. Fay, D. M. Small, J. Jaworski, J. S. Riley, D. Tegazzini, C. Fenning, D. S. Jones, P. G. Johnston, D. B. Longley and C. J. Scott, *Am. Soc. Gene Cell Ther.*, 2014, **22**, 2083–2092.
10 A. S. Greenberg, D. Avila, M. Hughes, A. Hughes, E. C. McKinney and M. F. Flajnik, *Nature*, 1995, **374**, 168–173.
11 C. Barelle, D. S. Gill and K. Charlton, Shark Novel Antigen Receptors—The Next Generation of Biologic Therapeutics?, in *Pharmaceutical Biotechnology. Advances in Experimental Medicine and Biology*, ed. C. A. Guzmán and G. Z. Feuerstein, Springer, New York, NY, 2009, vol. 655.
12 C. Barelle and A. Porter, *Antibodies*, 2015, **4**, 240–258.
13 S. D. Nuttall, U. V. Krishnan, L. Doughty, A. Nathanielsz, N. Ally, R. N. Pike, P. J. Hudson, A. A. Kortt and R. A. Irving, *FEBS Lett.*, 2002, **516**, 80–86.
14 R. L. Stanfield, H. Dooley, M. F. Flajnik and I. A. Wilson, *Science*, 2004, **305**, 1770–1774.
15 S. D. Nuttall, U. V. Krishnan, L. Doughty, K. Pearson, M. T. Ryan, N. J. Hoogenraad, M. Hattarki, J. A. Carmichael, R. A. Irving and P. J. Hudson, *Eur. J. Biochem.*, 2003, **270**, 3543–3554.
16 O. C. Ubah, J. Steven, M. Kovaleva, L. Ferguson, C. Barelle, A. J. R. Porter and C. J. Barelle, *Front. Immunol.*, 2017, **8**, 1780.
17 M. Kovaleva, K. Johnson, J. Steven, C. J. Barelle and A. Porter, *Front. Immunol.*, 2017, **8**, 1121.
18 M. R. Muller, K. Saunders, C. Grace, M. Jin, N. Piche-Nicholas, J. Steven, R. O'Dwyer, L. Wu, L. Khetemenee, Y. Vugmeyster, T. P. Hickling, L. Tchistiakova, S. Olland, D. Gill, A. Jensen and C. J. Barelle, *mAbs*, 2012, **4**, 673–685.
19 N. W. Gale, M. G. Dominguez, I. Noguera, L. Pan, V. Hughes, D. M. Valenzuela, A. J. Murphy, N. C. Adams, H. C. Lin, J. Holash, G. Thurston and G. D. Yancopoulos, *Proc. Natl. Acad. Sci. U. S. A.*, 2004, **101**, 15949–15954.
20 L. T. Krebs, J. R. Shutter, K. Tanigaki, T. Honjo, K. L. Stark and T. Gridley, *Genes Dev.*, 2004, **18**, 2469–2473.
21 M. Hellström, L.-K. Phng, J. J. Hofmann, E. Wallgard, L. Coultas, P. Lindblom, J. Alva, A.-K. Nilsson, L. Karlsson, N. Gaiano, K. Yoon, J. Rossant, M. L. Iruela-Arispe, M. Kalén, H. Gerhardt and C. Betsholtz, *Nature*, 2007, **445**, 776–780.
22 R. Riahi, J. Sun, S. Wang, M. Long, D. D. Zhang and P. K. Wong, *Nat. Commun.*, 2015, **6**, 6556.
23 B. L. Krock, N. Skuli and M. C. Simon, *Genes Cancer*, 2011, **2**, 1117–1133.
24 M. Hellström, L.-K. Phng, J. J. Hofmann, E. Wallgard, L. Coultas, P. Lindblom, J. Alva, A.-K. Nilsson, L. Karlsson, N. Gaiano, K. Yoon, J. Rossant, M. L. Iruela-Arispe, M. Kalén, H. Gerhardt and C. Betsholtz, *Nature*, 2007, **445**, 776–780.
25 R. J. Suckling, B. Korona, P. Whiteman, C. Chillakuri, L. Holt, P. A. Handford and S. M. Lea, *EMBO J.*, 2017, **36**, 2204–2215.
26 N. S. Patel, M. S. Dobbie, M. Rochester, G. Steers, R. Poulsom, K. Le Monnier, D. W. Cranston, J. L. Li and A. L. Harris, *Clin. Cancer Res.*, 2006, **12**, 4836–4844.
27 A. M. Jubb, E. J. Soilleux, H. Turley, G. Steers, A. Parker, I. Low, J. Blades, J. L. Li, P. Allen, R. Leek, I. Noguera-Troise, K. C. Gatter, G. Thurston and A. L. Harris, *Am. J. Pathol.*, 2010, **176**, 2019–2028.
28 A. M. Jubb, H. Turley, H. C. Moeller, G. Steers, C. Han, J. L. Li, R. Leek, E. Y. Tan, B. Singh, N. J. Mortensen, I. Noguera-Troise, F. Pezzella, K. C. Gatter, G. Thurston, S. B. Fox and A. L. Harris, *Br. J. Cancer*, 2009, **101**, 1749–1757.
29 N. S. Patel, J.-L. Li, D. Generali, R. Poulsom, D. W. Cranston and A. L. Harris, *Cancer Res.*, 2005, **65**, 8690–8697.
30 Z. Li, J. Wang, L. Gong, Z. Wen, C. Xu and X. Huang, *Asian Pac. J. Cancer Prev.*, 2011, **12**(1), 215–218.
31 A. Drouillard, F. Puleo, J. B. Bachet, S. Ouazzani, A. Calomme, P. Demetter, G. Verset, J. L. Van Laethem and R. Maréchal, *Br. J. Cancer*, 2016, **115**(10), 1245–1252.
32 L. Zhou, L. Yu, G. Ding, W. Chen, S. Zheng and L. Cao, *Pathol. Oncol. Res.*, 2015, **21**, 1141–1147.
33 H.-T. Chen, Q.-C. Cai, J.-M. Zheng, X.-H. Man, H. Jiang, B. Song, G. Jin, W. Zhu and Z.-S. Li, *Ann. Surg. Oncol.*, 2012, **19**, 464–474.
34 S.-F. Huang, Z.-L. Yang, D.-Q. Li, Z.-Y. Liu, C.-W. Wang, X.-Y. Miao, Q. Zou and Y. Yuan, *Hepatobiliary Pancreat. Dis. Int.*, 2016, **15**, 640–646.
35 J. Ridgway, G. Zhang, Y. Wu, S. Stawicki, W.-C. Liang, Y. Chanthery, J. Kowalski, R. J. Watts, C. Callahan, I. Kasman, M. Singh, M. Chien, C. Tan, J.-A. S. Hongo, F. de Sauvage, G. Plowman and M. Yan, *Nature*, 2006, **444**, 1083–1087.
36 W.-C. Yen, M. M. Fischer, M. Hynes, J. Wu, E. Kim, L. Beviglia, V. P. Yeung, X. Song, A. M. Kapoun, J. Lewicki, A. Gurney, D. M. Simeone and T. Hoey, *Clin. Cancer Res.*, 2012, **18**, 5374–5386.
37 N. Takebe, D. Nguyen and S. X. Yang, *Pharmacol. Ther.*, 2014, **141**, 140–149.
38 M. Yan, C. A. Callahan, J. C. Beyer, K. P. Allamneni, G. Zhang, J. B. Ridgway, K. Niessen and G. D. Plowman, *Nature*, 2010, **463**, E6–E7.
39 L. Mendonça, A. Trindade, C. Carvalho, J. Correia, M. Badenes, J. Gigante and A. Duarte, *Clin. Exp. Metastasis*, 2019, **36**, 365–380.
40 G. Cotton, J. Thom, P. Trumper, S. Bell, A. Kamenski, M. Wappett, C. Barelle, M. Kovaleva, J. Steven, A. Porter, E. McLean, C. Saladino, A. McCann, A. Cranston and T. Harrison, *Cancer Res.*, 2019, **79**(13 Supplement), 222.
41 I. Noguera-Troise, C. Daly, N. J. Papadopoulos, S. Coetzee, P. Boland, N. W. Gale, H. C. Lin, G. D. Yancopoulos and G. Thurston, *Nature*, 2006, **444**, 1032–1037.
42 J. C. F. Nogueira, M. K. Greene, D. A. Richards, A. O. Furby, J. Steven, A. Porter, C. Barelle, C. J. Scott and V. Chudasama, *Chem. Commun.*, 2019, **55**, 7671–7674.

43 A. Harbuzariu, A. Rampoldi, D. S. Daley-Brown, P. Candelaria, T. L. Harmon, C. C. Lipsey, D. J. Beech, A. Quarshie, G. O. Ilies and R. R. Gonzalez-Perez, *Oncotarget*, 2017, **8**(5), 7740–7752.
44 H.-Y. Song, Y. Wang, H. Lan and Y.-X. Zhang, *Exp. Ther. Med.*, 2018, **16**, 53–60.
45 R. Straubinger, K. Hong, D. Friend and D. Papahadjopoulos, *Cell*, 1983, **32**, 1069–1079.
46 H. Diez, A. Fischer, A. Winkler, C. J. Hu, A. K. Hatzopoulos, G. Breier and M. Gessler, *Exp. Cell Res.*, 2007, **313**, 1–9.
47 J. H. Min, C. H. Lee, Y. W. Ji, A. Yeo, H. Noh, I. Song, E. K. Kim and H. K. Lee, *PLoS One*, 2016, **11**, e0147846.
48 L. Winters, N. Thambi, J. Andreev and F. Kuhnert, *Bio-protocol.*, 2016, **6**, e1947.